Open access • Journal Article • DOI:10.1109/TED.2016.2598793

Universal Compact Model for Organic Solar Cell — Source link

Jong W. Jin, Sungyeop Jung, Yvan Bonnassieux, Gilles Horowitz ...+4 more authors

Institutions: Centre national de la recherche scientifique, Aristotle University of Thessaloniki

Published on: 24 Aug 2016 - IEEE Transactions on Electron Devices (IEEE)

Topics: Organic solar cell and Photocurrent

Universal Compact Model for Organic Solar Cell

Jong W. Jin, Sungyeop Jung, Yvan Bonnassieux, Gilles Horowitz, Alexandra Stamateri, Christos Kapnopoulos, Argiris Laskarakis, and Stergios Logothetidis

***Abstract*— Accurate description of the electrical behavior of organic solar cells (OSCs) becomes necessary with the advance of OSC technology toward up-scaled modules. We propose here a compact model for OSCs, by identifying different regimes present in the device operation in dark and under light: OFF, exponential sub-V_{ON}, power-law above-V_{ON}, and photocurrent. We also present a complete parameter extraction method for the model. In addition, we discuss the effect of the resistivity of transparent electrode and the device size on the OSC performance, by illustrating expected modifications on the current–voltage curve and parameter values.**

***Index Terms*— Compact model, large-area solar cell, organic photovoltaics, organic solar cell (OSC).**

I. Introduction

ORGANIC electronics is a technological field attracting intense research efforts and wide industrial investments. Besides organic light-emitting diodes already intensively commercialized, organic solar cells (OSCs) has gained large attention due to tailorable material properties and compatibility with solution process, demonstrating the potential to reduce material and manufacturing costs [1], [2].

Important advances have been achieved in OSC device physics because of extensive studies on physical phenomena related to exciton and bulk-heterojunction, and the impact of each of the material and interface properties on OSC performances [3]–[6]. Models delivered by these works are in general differential equations, to be coupled with many other equations, such as Poisson and carrier continuity. This differential equation system can be numerically solved by, for example, finite element methods, thus, predicting OSC device behavior and giving information on physical quantities at each point inside device. On the other hand, with the advance of OSC technology from single cell to up-scaled modules [7]–[10], multiple-device simulation becomes necessary in order to predict module performance and consequently to find the module design allowing maximum power output. To enable such a simulation without excessive computational cost, simplified models able to accurately describe the electrical behavior of OSCs are necessary. This type of modeling is called "compact."

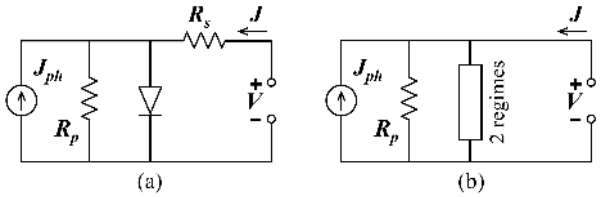

Fig. 1. (a) Classical four-element equivalent circuit model for solar cell, with diode, current source ($J_{\rm ph}$), shunt resistance (R_p), and series resistance (R_s). (b) Representation of the proposed compact model as a circuit. The device labeled "2 regimes" represents the sub-V_{ON} and above-V_{ON} regimes.

The classical approach for the compact modeling of solar cells is so-called equivalent circuit model. The most typical example contains four circuit elements, as shown in Fig. 1(a): diode, current source $J_{\rm ph}$, shunt resistance R_p, and series resistance R_s [11]. This model has the universal characteristic, in the sense that it is used regardless of material and structure employed, by describing the typical shape of the current density–voltage (J–V) curve of solar cell devices. The fitting quality is limited due to its simplicity, thus modified circuits with additional or alternative elements are often used [12]–[14].

Although the idea is simple, equivalent circuit models result in, when translated into mathematical equation, the current expressed as a function of current itself. This transcendental formulation makes difficult analytical treatments and parameter extraction. Mathematical methods have been proposed to enable analytical solving of the four-element equivalent circuit equation [15], [16], but they are limited to a specific circuit model. In this regard, compact models with nontranscendental formulation have been proposed [17], [18]. To assess such models, we point out three aspects: easy use, fitting quality, and attribution of physical meaning to the parameters.

The last aspect requires a particular attention in solar cell modeling. In this device, the charge carriers are transported in the direction parallel to the photoactive surface by the transparent electrode, which has a nonnegligible sheet resistance. One of the most basic requirements for solar cells is the large photoactive area; however, in a large-area device, the resistance of the electrode can severely decrease the power output and modify J–V curve [11], [19]–[22]. As a result, the parameter values of a model depend not only on material or interface prop-

Manuscript received June 2, 2016; revised July 29, 2016; accepted August 6, 2016. This work was supported by the European Union Seventh Framework Program (FP7/2007-2013) under Grant 310229 (SMARTONICS Project). The review of this paper was arranged by Editor A. G. Aberle.

J. W. Jin, S. Jung, Y. Bonnassieux, and G. Horowitz are with the Laboratoire de Physique des Interfaces et des Couches Minces, Centre National de la Recherche Scientifique, École Polytechnique, Université Paris-Saclay, 91128 Palaiseau, France (e-mail: jong.jin@polytechnique.edu; sungyeop.jung@polytechnique.edu; yvan.bonnassieux@polytechnique.edu; gilles.horowitz@polytechnique.edu).

A. Stamateri, C. Kapnopoulos, A. Laskarakis, and S. Logothetidis are with the Laboratory for Thin Films-Nanobiomaterials-Nanosystems and Nanometrology, Department of Physics, Aristotle University of Thessaloniki, 54124 Thessaloniki, Greece (e-mail: astama@physics.auth.gr; chkapnop@auth.gr; alask@auth.gr; logot@auth.gr).

Color versions of one or more of the figures in this paper are available online at http://ieeexplore.ieee.org.

Digital Object Identifier 10.1109/TED.2016.2598793

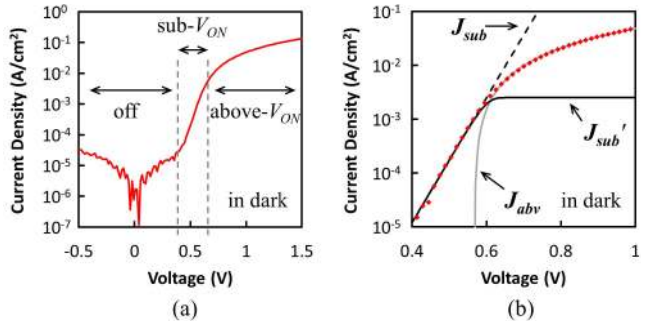

Fig. 2. (a) Three regimes in dark J–V curve: OFF, exponential sub-V_{ON}, and power-law above-V_{ON}. (b) Behavior of J'_{sub} function; it follows J_{sub} if J_{sub} is lower than the defined parameter J_{tr}, and it rapidly converges to J_{tr} when J_{sub} becomes higher than J_{tr}. Red plots (line and scatter): experimental dark J–V data (the same data of Section III).

erties but also on the device size. Therefore, it is important to know how this size effect is translated in the parameter values.

In this paper, we propose a compact model with new approach, dividing J–V curve in three regimes in dark, namely, OFF, sub-V_{ON} and above-V_{ON}, in addition to the photocurrent. The model is presented in Section II, followed by the complete parameter extraction method and fitting examples in Section III. The large-area feature is considered in Section IV, pointing out the effect of the device size on the parameter values.

II. Compact Model

A. OSC in Dark

In the proposed model, we divide the behavior of OSC in dark into three different regimes: OFF, sub-V_{ON} and above-V_{ON}, as shown in Fig. 2(a). To facilitate the comparison with four-element equivalent circuit model, the proposed model is schematized as an equivalent circuit in Fig. 1(b), with the device labeled "2 regimes" representing the sub-V_{ON} and above-V_{ON} regimes combined.

The sub-V_{ON} regime indicates the range of voltage, where we observe an exponential J–V curve. We have adopted the name "sub-V_{ON}" in order to distinguish this regime from the other one, where the device shows much higher current with nonexponential behavior. Note that, when plotted in linear scale, the sub-V_{ON} current appears practically as zero. The OFF regime is, as the name indicates, the part of J–V curve before the apparition of sub-V_{ON} current. We describe the current density in each regime (J_{OFF}, J_{sub}, and J_{abv}) as follows:

$$J_{OFF} = \frac{V}{R_p} \tag{1}$$

$$J_{sub} = J_0 \exp\left(\frac{qV}{nkT}\right) \tag{2}$$

$$J_{abv} = A(V - V_{ON})^{\gamma} \quad \text{if } V \geq V_{ON} \tag{3a}$$

$$J_{abv} = 0 \quad \text{if } V \leq V_{ON} \tag{3b}$$

and these equations are grouped in one function as follows:

$$J_{dark} = J_{OFF} + \left[\left\{J_{tr}\tanh\left(\frac{J_{sub}}{J_{tr}}\right)\right\}^m + J_{abv}^m\right]^{\frac{1}{m}}. \tag{4}$$

The OFF regime is modeled with one parameter, which is the shunt resistance R_p. The diode-like exponential curve of sub-V_{ON} current is described with two parameters, namely, saturation current density J_0 and ideality factor n. In (2), q is the elementary charge, k is the Boltzmann constant, and T is the temperature. Note that these two regimes are described in a similar way to the four-element equivalent circuit model. For the above-V_{ON} regime, we propose to use the power law with three parameters V_{ON}, γ, and A. This approach of dividing J–V curve into three regimes as well as the power law is common in the modeling of thin-film transistors (TFT) [23]–[25].

The individual equations need to be combined into one single expression with adequate treatment to describe the transition between regimes. However, as seen in Fig. 2(b), J_{sub} keeps increasing in the above-V_{ON} regime, and J_{abv} is zero for V lower than V_{ON}. This means that simple sum or sum of inverse of J_{sub} and J_{abv} cannot describe the transition between sub-V_{ON} and above-V_{ON} regimes. In order to overcome this issue, we define an auxiliary function J'_{sub} with a mathematical parameter J_{tr}, as follows:

$$J'_{sub} = J_{tr}\tanh\left(\frac{J_{sub}}{J_{tr}}\right). \tag{5}$$

The subscript tr stands for transition, and note that $J'_{sub} \approx J_{sub}$ if $J_{sub} < J_{tr}$, and $J'_{sub} \approx J_{tr}$ if $J_{sub} > J_{tr}$, as seen in Fig. 2(b). This function is summed with J_{abv} in root-sum-power form with another mathematical parameter m as in (4), which is a standard technique used to describe a transition between two regimes. Note that, if $m = 1$, (4) becomes a simple sum, and when the value of m is larger, the transition becomes more abrupt. In (4), J_{OFF} is simply summed, since this current is modeled as that of a resistance in parallel.

B. OSC Under Light

To describe J–V curve of OSC under light, we add the photocurrent term (J_{ph}) as follows:

$$J_{light} = J_{OFF} + \left[\left\{J_{tr}\tanh\left(\frac{J_{sub}}{J_{tr}}\right)\right\}^m + J_{abv}^m\right]^{\frac{1}{m}} - J_{ph}. \tag{6}$$

The function J_{ph} is modeled in the simplest way, *i.e.*, as a constant. The functions J_{OFF} and J_{abv} under light are modeled in the same way of the model for OSC in dark, *i.e.*, as (1) and (3). For J_{sub} under light, we propose to use double-exponential approach

$$J_{sub} = \left(J_{sub1}^{m_{sub}} + J_{sub2}^{m_{sub}}\right)^{\frac{1}{m_{sub}}} \tag{7}$$

where

$$J_{sub1} = J_{01}\exp\left(\frac{qV}{n_1kT}\right) \tag{8}$$

and

$$J_{sub2} = J_{02}\exp\left(\frac{qV}{n_2kT}\right). \tag{9}$$

We have chosen the double-exponential approach considering more practical aspects of model implementation than device physics. This choice improves the fitting quality without the use of nonfamiliar mathematical expressions. Parameters can be easily extracted, and also this approach is commonly used in

equivalent circuit models [12]–[14], [18], making the proposed model more accessible.

In Fig. 1(b), we note that the device labeled "2 regimes" substitutes the diode and series resistance. The series resistance is not explicitly expressed as one parameter in our model, since there are several factors influencing its value in the classical model. This point is discussed in detail in Section IV. Finally, we emphasize that, as we describe separately each regime and then group them into one function, the model can be easily modified if the fitting quality is insufficient in a particular range of voltage in case studies.

III. Parameter Extraction and Fitting Results

Once a compact model is designed, a systematic parameter extraction method has to be developed. In this section, we describe how the parameters of the proposed model can be extracted. The presented method is one of the possibilities; the aim of this section is to demonstrate that the model can be easily implemented. The device used as example in this section was fabricated on indium tin oxide (ITO)/glass substrate and includes 30 nm of poly(3,4-ethylenedioxythiophene):poly(styrenesulfonate) (PEDOT:PSS) layer, 200 nm of poly(3-hexylthiophene):phenyl-C_{61}-butyric acid methyl ester (P3HT:PCBM) photoactive layer, 10 nm of Ca, and 100 nm of Al, as schematized in Fig. 3(a). The organic layers were deposited by spin coating, and Ca and Al by thermal evaporation. The device has 0.06 cm^2 of photoactive area and was characterized in dark and under AM1.5G illumination.

A. OSC in Dark

The parameter R_p can be extracted with a simple linear fit in the OFF regime, as in Fig. 3(b). In Fig. 3, red scatters indicate the experimental data. Once J_{OFF} is defined, we subtract J_{OFF} from the experimental current density, and this curve is used to extract the two parameters of sub-V_{ON} regime (J_0 and n) with an exponential fit, as previously shown in Fig. 2(b).

The extraction method of power-law parameters is well established in the context of TFTs; here, we adopt the $H(V)$ function method presented in [25] and [26] to extract the parameters of the above-V_{ON} regime. $H(V)$ function is defined as the integral of the current density from V_{ON} to V divided by the current density at V

$$H(V) = \frac{\int_{V_{\text{ON}}}^{V} J(V')dV'}{J(V)}. \tag{10}$$

Since $J \approx J_{\text{abv}}$ when $V > V_{\text{ON}}$, the $H(V)$ function can be approximated as the integral of J_{abv} divided by J_{abv}, which results in a linear expression as follows:

$$H(V) \approx \frac{\int_{V_{\text{ON}}}^{V} J_{\text{abv}}(V')dV'}{J_{\text{abv}}(V)} = \frac{1}{\gamma+1}V - \frac{V_{\text{ON}}}{\gamma+1}. \tag{11}$$

Therefore, by plotting $H(V)$ as a function of V, a simple linear fit can extract two parameters V_{ON} and γ. Note that the integral is calculated from V_{ON}, which is an unknown quantity *a priori*. However, since the current near V_{ON} is several orders lower than the current at high voltage, the fact that the V_{ON} value is unknown does not affect significantly the extracted parameter values. For a more accurate extraction, a small number of iterations can be used to obtain a converged value for V_{ON}. The $H(V)$ function calculated from the experimental data is shown in Fig. 3(c). The most part of the graph shows a linear behavior, which indicates that the power law can successfully describe the current density in the above-V_{ON} regime. The remaining parameter A can be extracted by plotting the experimental current density as a function of $(V-V_{\text{ON}})^{\gamma}$, as shown in Fig. 3(d).

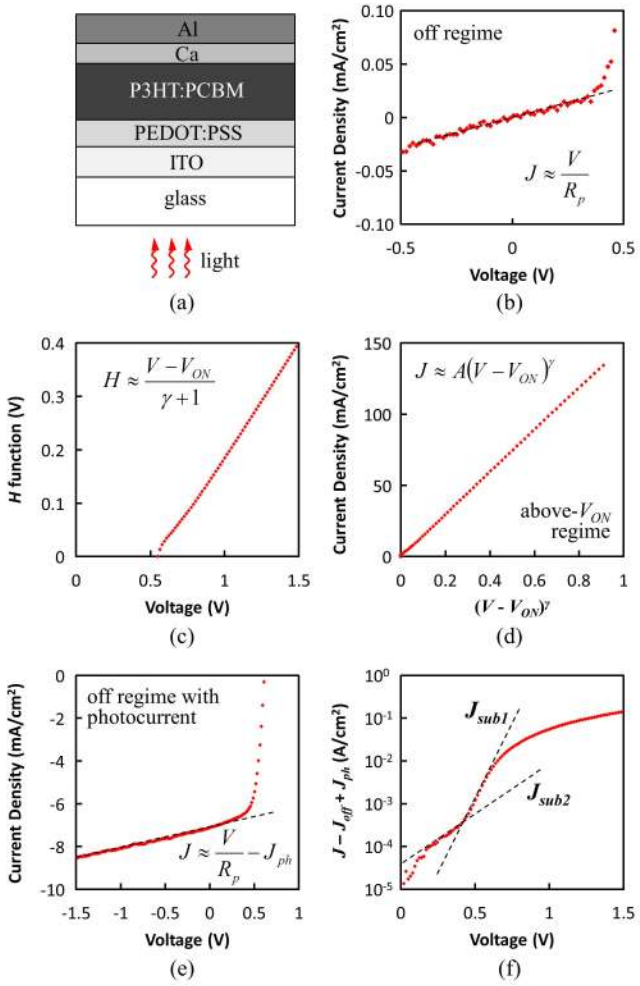

Fig. 3. (a) Structure of the OSC device used in the presentation of the parameter extraction method. (b) Extraction of the parameter R_p with a linear fit (black dotted line) in the OFF regime in dark. Red scatter plot: experimental data. (c) Extraction of V_{ON} and γ with a linear fit to H function. (d) Current density as a function of $(V-V_{\text{ON}})^{\gamma}$ to obtain A. (e) Extraction of R_p and J_{ph} with a linear fit in the OFF regime under light. (f) Extraction of parameters in J_{sub1} and J_{sub2} by plotting $J - J_{\text{OFF}} + J_{\text{ph}}$ in semilog scale.

Two remaining parameters (J_{tr} and m) are mathematical parameters. In general, $m = 4$ is a good choice, since it is mathematically simple and, at the same time, high enough to describe fast transition between sub- and above-V_{ON} regimes. The same choice is suggested for the parameter m_{sub} when double-exponential form is used for J_{sub}, as in (7). The parameter J_{tr} can be chosen in such a way that ensures both the fitting quality and smooth transition between regimes in terms of continuity and derivability. A good initial guess is the twice of J at $V = V_{\text{ON}}$

$$J_{\text{tr}} \approx 2J(V_{\text{ON}}). \tag{12}$$

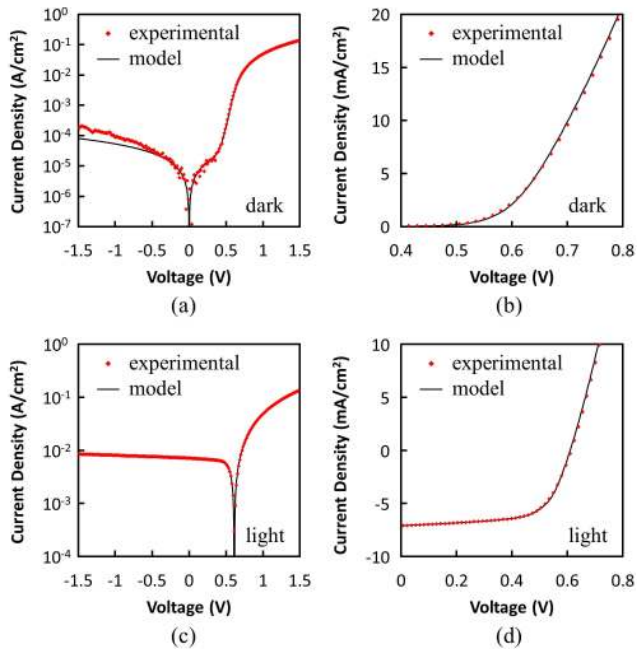

Fig. 4. Experimental J–V curve (red scatters) compared with the proposed compact model (black line) (a) in dark, in semilog scale, (b) in dark, in linear scale, (c) under light, in semilog scale, and (d) under light, in linear scale.

TABLE I
EXTRACTED PARAMETER VALUES

In dark		Under light (AM1.5)	
Parameter	Extracted value	Parameter	Extracted value
		J_{ph}	7.13×10^{-3} A/cm^2
R_p	1.88×10^4 Ω·cm^2	R_p	1.09×10^3 Ω·cm^2
n	1.46	n_1	2.33
J_0	2.69×10^{-10} A/cm^2	J_{01}	2.61×10^{-7} A/cm^2
		n_2	6.87
		J_{02}	3.17×10^{-5} A/cm^2
V_{ON}	0.57 V	V_{ON}	0.51 V
γ	1.34	γ	1.36
A	0.148 A/cm^2·V$^\gamma$	A	0.143 A/cm^2·V$^\gamma$
J_{tr}	2.5×10^{-3} A/cm^2	J_{tr}	4.1×10^{-3} A/cm^2

B. OSC Under Light

Since the model of OSC under light is very similar to that of OSC in dark, the parameter extraction method is also similar. The parameters $J_{\rm ph}$ and R_p can be extracted at the same time with a linear fit, as in Fig. 3(e). We eliminate $J_{\rm ph}$ and $J_{\rm OFF}$ from the experimental current density (*i.e.*, $J - J_{\rm OFF} + J_{\rm ph}$), and the obtained curve is used to extract all the remaining parameters. The sub-$V_{\rm ON}$ regime is fitted with two exponential curves, as shown in Fig. 3(f). For the parameters of above-$V_{\rm ON}$ regimes, $H(V)$ function can be used.

C. Fitting Results

The fitting results with the proposed model are compared with the experimental J–V curve in Fig. 4, in dark and under light, in linear and log scales. The extracted parameter values are shown in Table I. Note that the parameter values can depend on the light intensity. Except the OFF regime part, which is less relevant for the device operation, the model shows an outstanding fitting quality for all voltage range. Similar fitting quality was obtained in other devices: with P3HT:PCBM or P3HT:indene-C_{60} bisadduct (ICBA) as photoactive material, normal or inverted structure, device area from 0.06 to 0.70 cm^2, photoactive layer thickness from 100 to 350 nm, with or without metal nanoparticles inside PEDOT:PSS layer. This suggests that this model can be used for OSCs in general when no anomaly is present. Note that, since the proposed model is based on identifying three different regimes, devices showing s-shape behavior [27] are not described by the present model, and the parameter extraction may become difficult when the OFF-current is of the same order of magnitude as sub-$V_{\rm ON}$ current, or when the effect of the resistivity of transparent electrode is particularly high (discussed in Section IV).

IV. LARGE-SIZE CONSIDERATION

In this section, we study the effect of the solar cell size on the parameter values. First, we discuss the meaning of the series resistance in the equivalent circuit model. Then, we use 1-D distributed resistance model [20]–[22], taking into account the resistivity of the transparent conductor oxide (TCO), to obtain expected J–V curves for different device lengths and discuss the change observed on the parameter values.

When we describe J–V curve of a solar cell device with the classical four-element equivalent circuit approach [11], several factors contribute to the series resistance term. To make easier the presentation, here, we classify them into three categories: external, distributed, and intrinsic resistance. The external resistance is one that causes the difference between the externally applied voltage and the voltage actually applied on the active area of the device. Any type of resistance existing outside the photoactive area can be an example, such as interconnection or lumped element introduced by the measurement system. The distributed resistance is one that causes the nonuniformity of the voltage inside the photoactive area, such as the resistance of conductors (TCO and metal). Finally, the intrinsic resistance is one that makes deviation from the exponential diode curve even when other two counterparts do not exist. Injection barriers between layers and carrier transport in bulk material can be listed as the origin of the intrinsic resistance [28], [29].

All the three types of resistance modify J–V curve of a solar cell device. Using only one parameter (*e.g.*, series resistance in four-element equivalent circuit model) to represent all three types of resistance can result in an insufficient fitting quality, and it makes difficult the identification of the reason when a change on parameter values is observed. In mass production, where numerous devices are tested under a systematic quality assessment and failure analysis, it is of particular interest to be able to identify the effect of each of the resistance on the parameter values. The effect of the external resistance can be easily excluded from characterized J–V curve if this resistance value and the consequent voltage drop are known. However, the intrinsic and distributed resistance cannot be decoupled in a simple way.

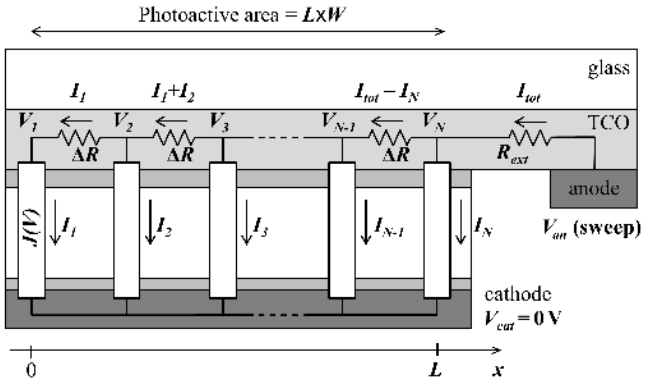

Fig. 5. Schematized 1-D distributed resistance model. External resistance is represented by R_{ext}, and ΔR indicates the distributed resistance in TCO. Rectangles represent ideal solar cell devices with only intrinsic resistance.

In order to estimate the effect of the distributed resistance, we use 1-D distributed resistance model [20]–[22], schematized in Fig. 5. We divide the photoactive area into N cells in parallel with device length Δx, and we consider a small resistance of TCO (ΔR) between two adjacent cells. Here, the length is defined in the direction of the current flow inside TCO. Since the sheet resistance of TCO is several orders higher than that of the metallic electrode, we consider that the electric potential is uniform in the cathode. The external resistance is represented by R_{ext}, located between the anode and the boundary of the photoactive area. Here, anode is defined as the final destination of photogenerated holes. Denoting $J_{\text{id}}(V)$ the ideal current density without external and distributed resistances, the current in an individual cell (I_n) is written as

$$I_n = J_{\text{id}}(V_n - V_{\text{cat}})W\Delta x \tag{13}$$

where V_{cat} is the electric potential at the cathode (equal to zero), V_n is the electric potential at the other extremity of the nth cell, and W is the device width. I_n is positive when the current flows from anode to cathode. Note that the photocurrent is negative. Considering the potential drop across ΔR, V_n is written as follows:

$$V_n = V_{n-1} + \sum_{i=1}^{n-1} I_i \Delta R \tag{14}$$

and we express ΔR in terms of the sheet resistance of TCO (r_{SR})

$$\Delta R = \frac{\Delta x}{W} r_{\text{SR}}. \tag{15}$$

The current of the entire solar cell (I_{tot}) is simply the sum of individual I_ns

$$I_{\text{tot}} = \sum_{i=1}^{N} I_i \tag{16}$$

and the electric potential at the boundary of the photoactive area nearest the anode is

$$V_N = V_{N-1} + \sum_{i=1}^{N-1} I_i \Delta R = V_{\text{cat}} - I_{\text{tot}} R_{\text{ext}}. \tag{17}$$

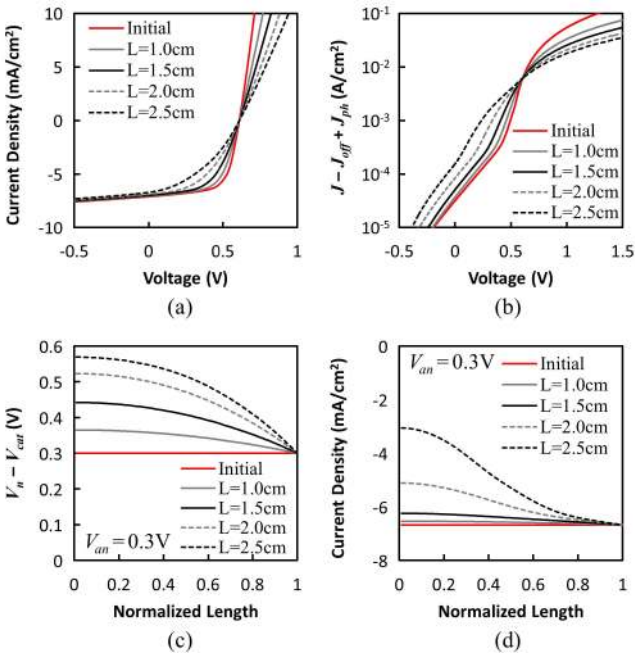

Fig. 6. Effect of the resistivity of TCO in devices with different length L, calculated with 1-D distributed resistance model, with the experimental data as the initial $J(V)$ function (red curve). (a) J–V curves. (b) J–V curves without photocurrent and OFF-regime current. (c) 1-D profile of the voltage applied to the device as a function of the position and (d) that of the current density.

When we numerically solve these equations for a given initial $J_{\text{id}}(V)$ function, we obtain 1-D profile of $V(x)$ and $I(x)$ as well as the J–V curve (resulting from I_{tot}) of the solar cell with nonnegligible TCO resistivity.

By varying the device length (L, from 1 to 2.5 cm), we calculated modified J–V curves, which are presented in Fig. 6(a). The ideal $J_{\text{id}}(V)$ function is unknown; here, we used, for example purposes, the function determined by (6) with the parameters of Table I as $J_{\text{id}}(V)$ function, although the effect of distributed and external resistances is not completely negligible in the experimental J–V curve. We specify that the size of the actual device is 0.06 cm^2 (L = 0.4 cm and W = 0.15 cm). For the sheet resistance, we used the experimental value r_{SR} = 20 Ω/□, and R_{ext} was chosen as zero to exclude the effect of the external resistance. We used the proposed compact model to describe the curves of Fig. 6(a), and the corresponding parameter values are shown in Table II. Note that, in the 1-D distributed resistance model, the J–V curve does not depend on W, and that doubling L is equivalent to multiplying the sheet resistance by four.

We can immediately see in Fig. 6(a) that, when we increase the device length, the fill factor (FF) decreases, with the photocurrent magnitude starting to decrease at lower V. In addition, when we eliminate J_{ph} and J_{OFF} from J and plot this quantity (*i.e.*, $J - J_{\text{OFF}} + J_{\text{ph}}$), as in Fig. 6(b), we observe that the curve appears more "stretched" in longer devices. Both behaviors can be interpreted as the transition between sub-V_{ON} and above-V_{ON} regimes happening in a broader range of voltage, which results directly from the nonuniform distribution of the electric potential inside TCO. This nonuniform distribution can be clearly observed in Fig. 6(c) and (d), which shows,

TABLE II
EXTRACTED PARAMETER VALUES

Parameter	L = 1.0 cm	L = 1.5 cm	L = 2.0 cm	L = 2.5 cm
J_{ph} (A/cm^2)	7.08×10^{-3}	7.02×10^{-3}	6.95×10^{-3}	6.85×10^{-3}
R_p (Ω·cm^2)	1.09×10^{3}	1.09×10^{3}	1.11×10^{3}	1.11×10^{3}
n_1	2.93	3.49	4.08	4.58
J_{01} (A/cm^2)	2.27×10^{-6}	1.05×10^{-5}	4.24×10^{-5}	1.46×10^{-4}
n_2	6.70	6.63	6.76	6.33
J_{02} (A/cm^2)	3.79×10^{-5}	5.11×10^{-5}	8.48×10^{-5}	1.58×10^{-4}
V_{ON} (V)	0.46	0.41	0.34	0.25
γ	1.25	1.27	1.31	1.38
A (A/cm^2·V$^{\gamma}$)	7.19×10^{-2}	4.89×10^{-2}	3.53×10^{-2}	2.64×10^{-2}
J_{tr} (A/cm^2)	3.0×10^{-3}	3.0×10^{-3}	2.5×10^{-3}	2.3×10^{-3}
V_{OC} (V)	0.61	0.61	0.61	0.61
FF (%)	60.3	54.2	46.3	39.4

The parameters corresponding to the initial $J(V)$ curve used to calculate other curves (with L from 1.0cm to 2.5cm) are those shown in Table I (under light), with FF of 65.3%.

for different device lengths and a given $V_{\rm an}$ value (0.3 V), the 1-D profile of the applied voltage (*i.e.*, $V_n - V_{\rm cat}$) and the current density in the nth device, respectively. In those figures, x-axis represents the position of the nth device, normalized with respect to the device length L; 0 and 1 mean, respectively, farthest from and nearest to the anode. The distribution of the voltage and current is more significant in devices with longer L, due to both higher total resistance of TCO (same resistivity but longer length) and higher total current (lower current density but larger area).

When TCO is a perfect conductor, there is no potential drop inside TCO, thus all I_n have the same value. However, when the resistivity of TCO is not zero, I_n varies as in (13), (14), and Fig. 6(d). As a result, a part of the OSC can be in a regime while the other part can be in another regime. For example, in devices with $L = 2$ or 2.5 cm of Fig. 6(c), V_n far from the anode is higher than $V_{\rm ON} = 0.51$ V of $J_{\rm id}(V)$, when the voltage applied to the anode is still below that value ($V_{\rm an} = 0.3$ V < 0.51 V). Since the current we measure at the terminal electrodes is the sum of all I_ns (*i.e.*, $I_{\rm tot}$), we observe, when compared with $J_{\rm id}(V)$, a smaller current, broader interregime transition, and lower $V_{\rm ON}$ value in devices with nonzero TCO resistivity. This size effect is well represented by the parameter values of the proposed compact model, as shown in Table II. The stretched exponential sub-$V_{\rm ON}$ curve is translated as the increase of J_{01} and n_1 values. $V_{\rm ON}$ decreases in longer devices because of the larger distribution of the electric potential inside TCO. By the same reason, the current density in the above-$V_{\rm ON}$ regime and consequently the parameter A decrease, and $J_{\rm ph}$ is slightly decreased as well.

The analysis of this section clearly shows that the resistivity of TCO is a key feature for the OSC performance and emphasizes the importance of the correct design of cells and modules. Moreover, the implementation of the proposed compact model in large devices is demonstrated. In devices with particularly large L, the broad interregime transition may hinder the parameter extraction, since the extraction requires identification of each regime in J–V curve. However, such devices are expected to have very low FF and power conversion efficiency, being of little interest for the module design.

V. CONCLUSION

In this paper, we have proposed universal compact model for OSC, which consists of identifying and individually describing different regimes present in OSC operation and then combining them into one equation. This model shows an excellent fitting quality and allows easy extraction of parameters and flexible modifications. In addition, the model was used in the study of the effect of the resistivity of TCO in large devices. The nonuniform voltage inside TCO results in a broad interregime transition, decreasing the FF of OSCs and modifying parameter values.

REFERENCES

[1] G. A. Chamberlain, "Organic solar cells: A review," *Solar Cells*, vol. 8, no. 1, pp. 47–83, Feb. 1983.

[2] S. Günes, H. Neugebauer, and N. S. Sariciftci, "Conjugated polymer-based organic solar cells," *Chem. Rev.*, vol. 107, no. 4, pp. 1324–1338, Apr. 2007.

[3] V. D. Mihailetchi, L. J. A. Koster, J. C. Hummelen, and P. W. M. Blom, "Photocurrent generation in polymer-fullerene bulk heterojunctions," *Phys. Rev. Lett.*, vol. 93, no. 21, p. 216601, Nov. 2004.

[4] L. J. A. Koster, E. C. P. Smits, V. D. Mihailetchi, and P. W. M. Blom, "Device model for the operation of polymer/fullerene bulk heterojunction solar cells," *Phys. Rev. B*, vol. 72, no. 8, p. 085205, Aug. 2005.

[5] F. Monestier *et al.*, "Modeling the short-circuit current density of polymer solar cells based on P3HT:PCBM blend," *Solar Energy Mater. Solar Cells*, vol. 91, no. 5, pp. 405–410, Mar. 2007.

[6] J. D. Servaites, M. A. Ratner, and T. J. Marks, "Organic solar cells: A new look at traditional models," *Energy Environ. Sci.*, vol. 4, no. 11, pp. 4410–4422, Nov. 2011.

[7] C. Lungenschmied *et al.*, "Flexible, long-lived, large-area, organic solar cells," *Solar Energy Mater. Solar Cells*, vol. 91, no. 5, pp. 379–384, Mar. 2007.

[8] F. C. Krebs, T. Tromholt, and M. Jørgensen, "Upscaling of polymer solar cell fabrication using full roll-to-roll processing," *Nanoscale*, vol. 2, no. 6, pp. 873–886, Jun. 2010.

[9] C. Koidis *et al.*, "Effect of process parameters on the morphology and nanostructure of roll-to-roll printed P3HT:PCBM thin films for organic photovoltaics," *Solar Energy Mater. Solar Cells*, vol. 112, pp. 36–46, May 2013.

[10] C.-H. Kim *et al.*, "Equivalent circuit modeling for a high-performance large-area organic photovoltaic module," *IEEE J. Photovolt.*, vol. 5, no. 4, pp. 1100–1105, Jul. 2015.

[11] M. B. Prince, "Silicon solar energy converters," *J. Appl. Phys.*, vol. 26, no. 5, pp. 534–540, May 1955.

[12] S. Yoo, B. Domercq, and B. Kippelen, "Intensity-dependent equivalent circuit parameters of organic solar cells based on pentacene and C_{60}," *J. Appl. Phys.*, vol. 97, no. 10, p. 103706, May 2005.

[13] A. Cheknane, H. S. Hilal, F. Djeffal, B. Benyoucef, and J.-P. Charles, "An equivalent circuit approach to organic solar cell modelling," *Microelectron. J.*, vol. 39, no. 10, pp. 1173–1180, Oct. 2008.

[14] A. Ortiz-Conde, F. J. García-Sánchez, J. Muci, and A. Sucre-González, "A review of diode and solar cell equivalent circuit model lumped parameter extraction procedures," *Facta Univ. Ser., Electron. Energetics*, vol. 27, no. 1, pp. 57–102, Mar. 2014.

[15] A. Ortiz-Conde and F. J. García-Sánchez, "Approximate analytical expression for equation of ideal diode with series and shunt resistances," *Electron. Lett.*, vol. 28, no. 21, pp. 1964–1965, Oct. 1992.

[16] A. Jain and A. Kapoor, "Exact analytical solutions of the parameters of real solar cells using Lambert W-function," *Solar Energy Mater. Solar Cells*, vol. 81, no. 2, pp. 269–277, Feb. 2004.

[17] M. Akbaba and M. A. A. Alattawi, "A new model for I–V characteristic of solar cell generators and its applications," *Solar Energy Mater. Solar Cells*, vol. 37, no. 2, pp. 123–132, May 1995.

[18] S. Karmalkar and H. Saleem, "The power law J–V model of an illuminated solar cell," *Solar Energy Mater. Solar Cells*, vol. 95, no. 4, pp. 1076–1084, Apr. 2011.

[19] M. Wolf, "Limitations and possibilities for improvement of photovoltaic solar energy converters: Part I: Considerations for earth's surface operations," *Proc. IRE*, vol. 48, no. 7, pp. 1246–1263, Jul. 1960.
[20] J. J. Wysocki, "Effect of series resistance on photovoltaic solar energy conversion," *RCA Rev.*, vol. 22, no. 1, pp. 57–70, Mar. 1961.
[21] M. Wolf and H. Rauschenbach, "Series resistance effects on solar cell measurements," *Adv. Energy Convers.*, vol. 3, no. 2, pp. 455–479, Apr./Jun. 1963.
[22] L. D. Nielsen, "Distributed series resistance effects in solar cells," *IEEE Trans. Electron Devices*, vol. 29, no. 5, pp. 821–827, May 1982.
[23] M. S. Shur, H. C. Slade, M. D. Jacunski, A. A. Owusu, and T. Ytterdal, "SPICE models for amorphous silicon and polysilicon thin film transistors," *J. Electrochem. Soc.*, vol. 144, no. 8, pp. 2833–2839, Aug. 1997.
[24] G. Horowitz, M. E. Hajlaoui, and R. Hajlaoui, "Temperature and gate voltage dependence of hole mobility in polycrystalline oligothiophene thin film transistors," *J. Appl. Phys.*, vol. 87, no. 9, pp. 4456–4463, May 2000.
[25] B. Iñiguez *et al.*, "Universal compact model for long- and short-channel thin-film transistors," *Solid-State Electron.*, vol. 52, no. 3, pp. 400–405, Mar. 2008.
[26] A. Cerdeira, M. Estrada, R. García, A. Ortiz-Conde, and F. J. García-Sánchez, "New procedure for the extraction of basic a-Si:H TFT model parameters in the linear and saturation regions," *Solid-State Electron.*, vol. 45, no. 7, pp. 1077–1080, Jul. 2001.
[27] A. Wagenpfahl, D. Rauh, M. Binder, C. Deibel, and V. Dyakonov, "S-shaped current-voltage characteristics of organic solar devices," *Phys. Rev. B.*, vol. 82, no. 11, p. 115306, Sep. 2010.
[28] P. W. M. Blom, M. J. M. de Jong, and J. J. M. Vleggaar, "Electron and hole transport in poly(*p*-phenylene vinylene) devices," *Appl. Phys. Lett.*, vol. 68, no. 23, pp. 3308–3310, Jun. 1996.
[29] P. S. Davids, I. H. Campbell, and D. L. Smith, "Device model for single carrier organic diodes," *J. Appl. Phys.*, vol. 82, no. 12, pp. 6319–6325, Dec. 1997.

Jong W. Jin received the B.Sc. degree in physics from the University of Sao Paulo, São Paulo, Brazil, the Diploma in Engineering degree from École Polytechnique, Palaiseau, France, and the Ph.D. degree from École Polytechnique in 2013, under a double degree agreement.

He is currently a Post-Doctoral Researcher with the Laboratoire de Physique des Interfaces et des Couches Minces, École Polytechnique.

Sungyeop Jung received the M.Eng. degree from Kyung Hee University, Seoul, South Korea, and the M.Sc. degree from École Polytechnique, Palaiseau, France, in 2013, through the Dual Degree Program, where he is currently pursuing the Ph.D. degree.

Yvan Bonnassieux received the Ph.D. degree from the École Normale Supérieure de Cachan, Cachan, France, in 1998.

He is currently a Professor with École Polytechnique, Palaiseau, France, where he is also the Head of the Organic Large Area Electronics Research Team, Laboratoire de Physique des Interfaces et des Couches Minces.

Gilles Horowitz received the Ph.D. degree from Paris Diderot University, Paris, France, in 1975.

He is currently an Emeritus Research Fellow with the Centre National de la Recherche Scientifique, Paris, France, and the Laboratoire de Physique des Interfaces et des Couches Minces, École Polytechnique, Palaiseau, France.

Alexandra Stamateri received the B.Sc. degree in physics and the M.Sc. (Diploma) degree in nanosciences and nanotechnologies from the Aristotle University of Thessaloniki, Thessaloniki, Greece, in 2015. She is currently pursuing the Ph.D. degree with the Laboratory for Thin Films-Nanobiomaterials-Nanosystems and Nanometrology, Thessaloniki.

Christos Kapnopoulos received the B.Sc. degree in physics and the M.Sc. (Diploma) degree in nanosciences and nanotechnologies from the Aristotle University of Thessaloniki, Thessaloniki, Greece, in 2012. He is currently pursuing the Ph.D. degree with the Laboratory for Thin Films-Nanobiomaterials-Nanosystems and Nanometrology, Thessaloniki.

Argiris Laskarakis received the Ph.D. degree from the Aristotle University of Thessaloniki, Thessaloniki, Greece, in 2005.

He is currently the Head of the Organic Electronics Group with the Laboratory for Thin Films-Nanobiomaterials-Nanosystems and Nanometrology, Department of Physics, Aristotle University of Thessaloniki.

Stergios Logothetidis received the Ph.D. degree from the Aristotle University of Thessaloniki, (AUTh), Thessaloniki, Greece, in 1984.

He is currently a Professor of Physics with the Physics Department, AUTh. He is also the Founder and the Director of the Laboratory for Thin Films-Nanobiomaterials-Nanosystems and Nanometrology and the Center for Organic and Printed Electronics–Hellas, the Chairman of the NANOTEXNOLOGY multi-event, and the President of Hellenic Organic and Printed Electronics Association.